LETTER

doi:10.1038/nature14218

Highly efficient star formation in NGC 5253 possibly from stream-fed accretion

J. L. Turner[1], S. C. Beck[2], D. J. Benford[3], S. M. Consiglio[1], P. T. P. Ho[4], A. Kovács[5], D. S. Meier[6,7] & J.-H. Zhao[8]

Gas clouds in present-day galaxies are inefficient at forming stars. Low star-formation efficiency is a critical parameter in galaxy evolution: it is why stars are still forming nearly 14 billion years after the Big Bang[1] and why star clusters generally do not survive their births, instead dispersing to form galactic disks or bulges[2]. Yet the existence of ancient massive bound star clusters (globular clusters) in the Milky Way suggests that efficiencies were higher when they formed ten billion years ago. A local dwarf galaxy, NGC 5253, has a young star cluster that provides an example of highly efficient star formation[3]. Here we report the detection of the $J = 3 \rightarrow 2$ rotational transition of CO at the location of the massive cluster. The gas cloud is hot, dense, quiescent and extremely dusty. Its gas-to-dust ratio is lower than the Galactic value, which we attribute to dust enrichment by the embedded star cluster. Its star-formation efficiency exceeds 50 per cent, tenfold that of clouds in the Milky Way. We suggest that high efficiency results from the force-feeding of star formation by a streamer of gas falling into the galaxy.

The Submillimeter Array image of NGC 5253, shown in Fig. 1, reveals a bright CO(3→2) source coincident with the giant cluster and its 'supernebula'[4]. 'Cloud D' (ref. 3) is one of only two molecular clouds detected within the galaxy; the second cloud is smaller and located ~5″ (90 pc) to the southwest. A 'streamer' of gas extending along the minor axis is also detected in CO(3→2). This streamer, previously detected in lower-J CO lines, seems to be falling into the galaxy near the supernebula[3,5]. Both the streamer and Cloud D emit 870-μm continuum emission, as shown in Fig. 2. Also shown is an image of 350-μm continuum, in which both Cloud D and the streamer are detected.

The molecular gas in Cloud D is hot. This is clear from the increase in brightness from CO(2→1) (ref. 3) to CO(3→2). The intensity ratio of the two lines is $I_{32}/I_{21} = 2.6 \pm 0.5 (I_{\rm line} = \int T_{\rm line}\,{\rm d}v)$. This ratio is non-thermal, although the thermal limit of 2.25 ($\sim \nu^2$) is within the uncertainties and is what we adopt. Non-local-thermodynamic-equilibrium (non-LTE) modelling of this ratio using RADEX[6] indicates a minimum kinetic temperature of $T_{\rm K} > 200$ K for the 1σ lower limit, and $T_{\rm K} > 350$ K for the adopted value of $I_{32}/I_{21} = 2.25$ (see Methods). The high gas temperature is consistent with a thermal origin for H_2 2.2-μm emission in the region[7]. Cloud D seems to be a photon-dominated region, heated by ultraviolet radiation from the several thousand cluster O stars in the cluster[4,8]. The CO(3→2)-emitting gas is dense, with $n_{\rm H_2} \approx (4.5 \pm 0.5) \times 10^4$ cm^{-3}.

By contrast with Cloud D, the streamer consists of more typical cool giant molecular clouds. Its value of $I_{32}/I_{21} = 1.0 \pm 0.3$ is consistent with optically thick emission, for which RADEX models allow temperatures as low as $T_{\rm K} \approx 15$–20 K, and number densities $n_{\rm H_2} \approx 3.5$–4×10^4 cm^{-3}. The mass of the streamer is $M_{\rm H_2} \approx 2 \times 10^6 M_\odot$[3], which is 1–2% of the stellar mass of the galaxy. The streamer is molecular, dense, and primed for star formation, even before entering the galaxy. This is unlikely to be a primordial collapsing filament[9], but is more probably previously enriched gas.

The star-formation efficiency of a cloud or region can be defined as $\eta = M_{\rm stars}/(M_{\rm gas} + M_{\rm stars})$, where $M_{\rm stars}$ is the stellar mass and $M_{\rm gas}$ the mass of molecular gas. $M_{\rm gas}$ can be hard to define for star-forming regions within giant molecular clouds, but the association of the isolated Cloud D with the supernebula gives us an opportunity to calculate η directly for the giant molecular cloud giving birth to this massive star cluster—if we can determine the mass of Cloud D.

CO is often used to estimate the mass of molecular gas, but this is unreliable in NGC 5253. Here we use the width of the CO line to determine a gas mass for Cloud D based on dynamical considerations. The CO linewidth is $\sigma = 9.2 \pm 0.6$ km s^{-1}, based on a Gaussian fit. The cloud dimensions, deconvolved from the beam, are $2.8'' \times 1.5'' \pm 0.1''$ (52 pc × 28 pc). The virial mass is $M_{\rm vir} < 1.8^{+0.2}_{-0.7} \times 10^6 M_\odot$ for Cloud D, with uncertainties due to the unknown internal mass distribution (see Methods).

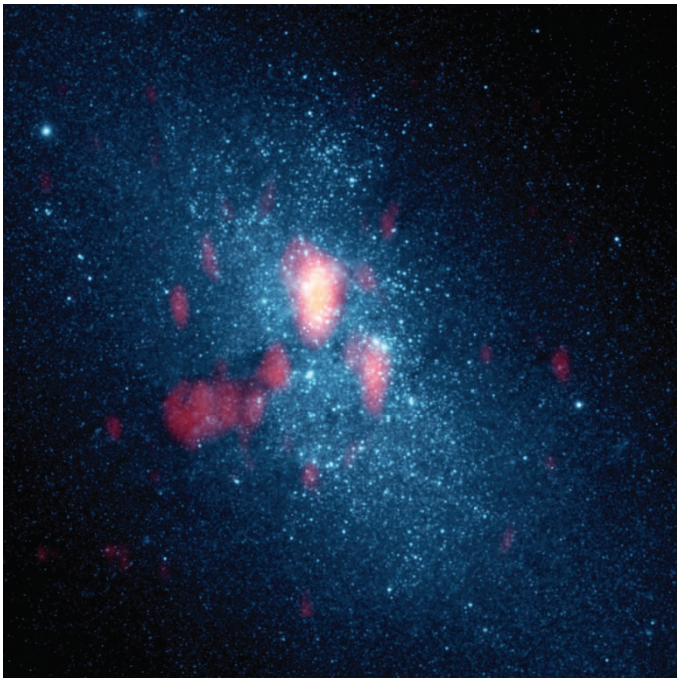

Figure 1 | CO $J = 3 \rightarrow 2$ emission in NGC 5253. The Submillimeter Array (SMA) CO(3→2) integrated line intensity, in red, is shown atop a λ814 nm Hubble Space Telescope image. The SMA beam is $4'' \times 2''$ (74 pc × 37 pc). The field covers $40'' \times 40''$ (740 pc × 740 pc), north up, east left. Image registration is to less than 1″. The CO streamer coincides with the optical dust lane to the east. The massive star cluster is located at the bright, compact CO peak, Cloud D; it is embedded[8,9] and is not visible here. Cloud F is to the southwest of Cloud D.

[1]Department of Physics and Astronomy, University of California, Los Angeles, Los Angeles, California 90095-1547, USA. [2]Department of Physics and Astronomy, University of Tel Aviv, 69978 Ramat Aviv, Israel. [3]Observational Cosmology Laboratory, Code 665, NASA at Goddard Space Flight Center, Greenbelt, Maryland 20771, USA. [4]Academia Sinica, Astronomy and Astrophysics, 11F Astronomy-Mathematics Building, AS/NTU No. 1, Sec. 4, Roosevelt Road, Taipei 10617, Taiwan. [5]Department of Physics, Caltech, Pasadena, California 91125, USA; Institute for Astrophysics, University of Minnesota, Minneapolis, Minnesota 55405, USA. [6]Department of Physics, New Mexico Institute of Mining and Technology, Socorro, New Mexico 85723, USA. [7]National Radio Astronomy Observatory, 1003 Lopezville Road, Socorro, New Mexico 85723, USA. [8]Harvard-Smithsonian Center for Astrophysics, 60 Garden Street, Cambridge, Massachusetts 02138, USA.

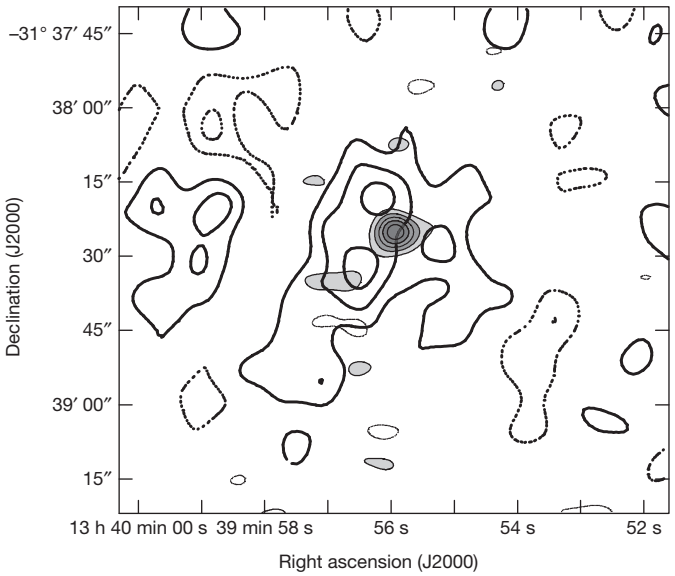

Figure 2 | Dust and gas in NGC 5253. SMA image of continuum dust emission at 870 μm (greyscale), with 350-μm dust continuum emission from SHARC at the Caltech Submillimeter Observatory (contours) superimposed. The SMA continuum image has been smoothed to 6″ resolution to show emission from the streamer. The SHARC image has been smoothed to 12.7″; contours are 2σ. Coordinates of the SHARC image are uncertain to ~5″ (see Methods).

We assume that the linewidth is gravitational, with no winds or outflow; this is therefore an upper limit to $M_{\rm vir}$. The virial mass includes both gas and stars, but we can constrain the stellar mass. The mass in stars exciting the supernebula, $M_{\rm stars}$, can be predicted from the Lyman continuum rate of $N_{\rm Lyc} = (7 \pm 2) \times 10^{52}\,{\rm s}^{-1}$ (ref. 6) and Bracket γ equivalent width of 255 Å (ref. 10). The star cluster has mass $M_{\rm stars} = 1.1^{+0.7}_{-0.2} \times 10^6 M_\odot$ (see Methods). We then obtain a gas mass $M_{\rm gas} = M_{\rm vir} - M_{\rm stars} = (7 \pm 4) \times 10^5 M_\odot$ if the cluster is embedded in the cloud. This treatment assumes that the CO kinematics trace all of the cloud and that there is no extensive layer of H_2 without CO; however, the dust continuum and CO sizes are nearly identical, consistent with the dust and gas mass being contained within Cloud D.

Other methods to estimate H_2 mass are problematic for Cloud D. CO(3→2) is optically thin, but the excitation temperature is not determined, nor is CO/H_2 known. The line strength of $41 \pm 8\,{\rm Jy\,km\,s}^{-1}$ gives $M_{\rm CO} = (4 \pm 1) M_\odot$ (T/200 K). For a Galactic abundance ratio of $[{\rm CO}]/[{\rm H_2}] = 8.5 \times 10^{-5}$, the H_2 mass would be $M_{\rm H_2} = 5 \times 10^4 M_\odot$ (T/200 K). This is one-tenth of the value for $M_{\rm gas}$ derived above. Intense radiation fields and high temperature will affect the chemistry and the relative abundance of CO.

Dust continuum emission can trace gas mass, but it is also unreliable in Cloud D. The 870-μm continuum flux density for Cloud D is $S_{870\mu{\rm m}} = 72 \pm 10$ mJy, consistent with previous measurements[11], of which free-free emission[8] contributes $S^{\rm ff}_{870\mu m} = 38 \pm 4$ mJy, leaving dust emission $S^{\rm dust}_{870\mu m} = 34 \pm 14$ mJy. Our 350-μm image gives $S^{\rm dust}_{350\mu m} = 1.0 \pm 0.2$ Jy for Cloud D, consistent with the 870-μm flux. Adopting the dust opacity of the Large Magellanic Cloud[12] (see Methods), we find an observed dust mass, $M_{\rm dust} = (1.5 \pm 0.2) \times 10^4 M_\odot\,({\rm T}/45\,{\rm K})^{-1}$. To obtain gas mass, we need a gas-to-dust ratio (GTD). Scaled as the oxygen abundance of NGC 5253, 0.2–0.3 solar[13,14], GTD ≈ 650, within the range 340–1,200 inferred for the Magellanic clouds[15–17]. The observed dust mass is fivefold the ~3,000$M_\odot$ of dust expected for a $2 \times 10^6 M_\odot$ gas cloud at GTD = 650. If instead we compare the observed dust mass with the dynamical estimate of gas mass, we derive GTD ≈ 47 for the embedded cluster, and in the unlikely case that the cluster is not embedded, GTD ≈ 120. Dust is an expected result of mass loss from massive, short-lived stars. Stellar models indicate that a cluster of massive stars of age 4.4 Myr, consistent with recombination line equivalent widths, will expel 20,000–30,000$M_\odot$ of elements carbon, oxygen, silicon, magnesium and iron depending on the cluster mass and initial mass function, of which ~30–50% will be in the form of dust (see Methods). To produce the amounts of dust and ionizing photons observed, given the upper limit imposed by the dynamical mass, suggests that the stellar initial mass function is top-heavy, with a lower mass cutoff of at least 2–3$M_\odot$ (see Methods.) The star cluster has probably produced most of the dust. To infer a gas mass on the basis of the observed dust emission for Cloud D from a GTD scaled to the global metallicity of NGC 5253 without accounting for *in situ* dust production, as has been done for other galaxies[18], would give an erroneously high gas mass and underestimate the star-formation efficiency.

Given the peculiarities of Cloud D, the most reliable gas mass is dynamical. We use this mass to calculate the star-formation efficiency, η. A lower limit to η occurs if the gravitational mass is all gas—no stars—so that $\eta = 1.1^{+0.7}_{-0.2} \times 10^6 M_\odot / (1.1^{+0.7}_{-0.2} + 1.8^{+0.2}_{-0.7}) \times 10^6 M_\odot \approx 38^{+24}_{-7}\%$. Even in this case, η significantly exceeds the $\eta < 1\%$ of Galactic giant molecular clouds and the highest efficiencies of $\eta \approx 15$–20% seen in individual cloud cores[19] in the Galaxy. However, it is almost certain that the star cluster is located within the cloud, given the subarcsecond positional coincidence of nebular emission and CO, the precise kinematic coincidence of nebular H53α (ref. 8) and CO line centroids, and the high extinction to the cluster. Thus the stellar mass also contributes to the linewidth. For the more realistic case that the cluster is embedded within Cloud D, $\eta = (1.1^{+0.7}_{-0.2}) \times 10^6 M_\odot / 1.8^{+0.2}_{-0.7} \times 10^6 M_\odot = 61^{+84}_{-16}\%$. This value exceeds even the canonical ~50% (see Methods) needed to allow a star cluster to survive in its current bound state with rapid gas dispersal. If dust competes with gas for ultraviolet photons, the Lyman continuum rate and stellar mass have been underestimated, and η is even higher. If there are winds or outflows contributing to the CO linewidth, η is higher. The large dust mass favours larger-mass cluster models for which η is higher. These values for η are uncertain, but they are free of the systematics due to standard assumptions such as gas-to-dust ratio, relative CO abundance or CO conversion factor. The star-formation efficiency of Cloud D is unusually high, implying gas consumption timescales of ~10 Myr.

A measurement of star-formation efficiency is a snapshot in time; η could be high because the gas has been incorporated into stars or because the young stars have already dispersed the gas. How and when a young star cluster disperses its gas is crucial to its survival[2,20]. For Cloud D, gas dispersal models are strongly constrained by the youth of the embedded star cluster[10], its positional coincidence with the cloud, lack of evidence for supernovae[21], and small CO(3→2) linewidth. Apparently not much has yet escaped this cloud.

Cloud D is a strange molecular cloud: hot, dusty, and small in mass relative to its young star cluster. It is found in a dark-matter-dominated galaxy. Its unusual properties may indicate a mode of star formation different from that observed in disk galaxies, including luminous infrared galaxies. Models of stochastic star formation for turbulently supported giant molecular clouds in our Galaxy suggest that star-formation efficiencies are 1% in a free-fall time[22], which implies that the ultimate efficiency can be limited if star formation is quenched by massive stellar feedback. An extended period of star formation might be facilitated if Cloud D is compressed by an external influence, as for example by a streamer of gas force-fed into the star-forming region by the galactic potential. Our data in NGC 5253 could support such a model. The streamer contains $\sim 2 \times 10^6 M_\odot$ of gas extending ~200–300 pc along the minor axis, entering the galaxy at a rate of ~20 pc Myr^{-1}. The streamer can fuel star formation at the present rate of ~0.1–0.2$M_\odot$ yr^{-1} for the next 10 Myr. This dwarf spheroidal galaxy is not rotationally supported[23]; multiple accreting streams from its extensive H I halo[24,25] could be responsible for its global dynamics and morphology[26] as well as its spheroidal system of massive star clusters spanning billions of years in age[27–29]. NGC 5253 may illustrate a new mode of highly efficient star cluster formation triggered by cold-stream accretion[30].

Online Content Methods, along with any additional Extended Data display items and Source Data, are available in the online version of the paper; references unique to these sections appear only in the online paper.

Received 28 July 2014; accepted 6 January 2015.

1. Kennicutt, R. C. Jr. The global Schmidt Law in star-forming galaxies. *Astrophys. J.* **498,** 541–552 (1998).
2. Bastian, N. & Goodwin, S. P. Evidence for the strong effect of gas removal on the internal structure of young stellar clusters. *Mon. Not. R. Astron. Soc.* **369,** L9–L13 (2006).
3. Meier, D. S., Turner, J. L. & Beck, S. C. Molecular gas and the young starburst in NGC 5253 revisited. *Astron. J.* **124,** 877–885 (2002).
4. Turner, J. L., Beck, S. C. & Ho, P. T. P. The radio supernebula in NGC 5253. *Astrophys. J.* **532,** L109–L112 (2000).
5. Turner, J. L., Beck, S. C. & Hurt, R. L. A. CO map of the dwarf starburst galaxy NGC 5253. *Astrophys. J.* **474,** L11–L14 (1997).
6. van der Tak, F. F. S., Black, J. H., Schöier, F. L., Jansen, D. J. & van Dishoeck, E. F. A computer program for fast non-LTE analysis of interstellar line spectra. With diagnostic plots to interpret the line intensity ratios. *Astron. Astrophys.* **468,** 627–635 (2007).
7. Cresci, G., Vanzi, L., Sauvage, M., Santagelo, G. & van der Werf, P. Integral-field near-infrared spectroscopy of two blue dwarf galaxies: NGC 5253 and He 2–10. *Astron. Astrophys.* **520,** A82 (2010).
8. Rodríguez-Rico, C. A., Goss, W. M., Turner, J. L. & Gómez, Y. VLA H53α observations of the central region of the super star cluster galaxy NGC 5253. *Astrophys. J.* **670,** 295–300 (2007).
9. Gray, W. J. & Scannapieco, E. Thermal and chemical evolution of collapsing filaments. *Astrophys. J.* **768,** 174 (2013).
10. Alonso-Herrero, A. *et al.* Obscured star formation in the central region of the dwarf galaxy NGC 5253. *Astrophys. J.* **612,** 222–237 (2004).
11. Hirashita, H. Properties of free-free, dust and CO emissions in the starbursts of blue compact dwarf galaxies. *Mon. Not. R. Astron. Soc.* **429,** 3390–3401 (2013).
12. Galliano, F. *et al.* Non-standard grain properties, dark gas reservoir, and extended submillimeter excess, probed by Herschel in the Large Magellanic Cloud. *Astron. Astrophys.* **536,** A88 (2011).
13. Kobulnicky, H. A., Skillman, E. D., Roy, J.-R., Walsh, J. R. & Rosa, M. R. HST FOS spectroscopy of localized chemical enrichment from massive stars in NGC 5253. *Astrophys. J.* **477,** 679–692 (1997).
14. López-Sánchez, Á. R., Esteban, C., García-Rojas, J., Peimbert, M. & Rodríguez, M. The localized chemical pollution in NGC 5235 revisited: results from deep echelle spectrophotometry. *Astrophys. J.* **656,** 168–185 (2007).
15. Bot, C., Boulanger, F., Lagache, G., Cambrésy, L. & Egret, D. Multi-wavelength analysis of the dust emission in the Small Magellanic Cloud. *Astron. Astrophys.* **423,** 567–577 (2004).
16. Gordon, K. *et al.* The dust-to-gas ratio in the Small Magellanic Cloud tail. *Astrophys. J.* **690,** L76–L80 (2009).
17. Roman-Duval, J. *et al.* Dust/gas correlations from Herschel observations. *Astron. Astrophys.* **518,** L74 (2010).
18. Shi, Y. *et al.* Inefficient star formation in extremely metal poor galaxies. *Nature* **514,** 335–338 (2014).
19. Olmi, L. & Testi, L. Constraints on star formation theories from the Serpens molecular cloud and protocluster. *Astron. Astrophys.* **392,** 1053–1068 (2002).
20. Smith, R., Goodwin, S., Fellhauer, M. & Assmann, P. Infant mortality in the hierarchical merging scenario: dependence on gas expulsion time-scales. *Mon. Not. R. Astron. Soc.* **428,** 1303–1311 (2013).
21. Beck, S. C., Turner, J. L., Ho, P. T. P., Lacy, J. H. & Kelly, D. M. The central star cluster of the star-forming dwarf galaxy NGC 5253. *Astrophys. J.* **457,** 610–615 (1996).
22. Krumholz, M. R. & McKee, C. F. A general theory of turbulence-regulated star formation, from spirals to ultraluminous infrared galaxies. *Astrophys. J.* **630,** 250–268 (2005).
23. Caldwell, N. & Phillips, M. M. Star formation in NGC 5253. *Astrophys. J.* **338,** 789–803 (1989).
24. Kobulnicky, H. A. & Skillman, E. D. Inflows and outflows in the dwarf starburst galaxy NGC 5253: high-resolution HI observations. *Astron. J.* **135,** 527–537 (2008).
25. López-Sánchez, Á. R. *et al.* The intriguing HI gas in NGC 5253: an infall of a diffuse, low-metallicity HI cloud? *Mon. Not. R. Astron. Soc.* **419,** 1051–1069 (2012).
26. Cen, R. Evolution of cold streams and the emergence of the Hubble sequence. *Astrophys. J.* **789,** L21 (2014).
27. Harris, J., Calzetti, D., Gallagher, J. S., Smith, D. A. & Conselice, C. J. The recent cluster formation histories of NGC 5253 and NGC 3077: environmental impact on star formation. *Astrophys. J.* **603,** 503–522 (2004).
28. Cresci, G., Vanzi, L. & Sauvage, M. The star cluster population of NGC 5253. *Astron. Astrophys.* **433,** 447–454 (2005).
29. de Grijs, R., Anders, P., Zackrisson, E. & Göran, Ö. The NGC 5253 star cluster system. I. Standard modelling and infrared-excess. *Mon. Not. R. Astron. Soc.* **431,** 2917–2932 (2013).
30. Dekel, A. *et al.* Cold streams in early massive hot haloes as the main mode of galaxy formation. *Nature* **457,** 451–454 (2009).

Acknowledgements We thank J. Carpenter, S. Goodwin, M. Heyer, L. Hunt, R. Hurt, M. Jura, C. Lada, C. Leitherer and S. Van Dyk for assistance with the analysis. The Submillimeter Array is a joint project between the Smithsonian Astrophysical Observatory and the Academia Sinica Institute of Astronomy and Astrophysics and is funded by the Smithsonian Institution and the Academica Sinica.

Author Contributions J.L.T., S.C.B., D.J.B., A.K. and D.S.M. performed the observations. J.L.T., S.C.B. and P.T.P.H. conceived the project and wrote the observing proposal. J.-H.Z. reduced and imaged the Submillimeter Array 870-μm data; A.K. reduced, imaged and analysed the SHARC 350-μm data. J.L.T. and S.M.C. obtained derived quantities and performed data analysis. J.L.T. wrote the first draft and constructed figures. All authors read, discussed and commented on the draft.

Author Information Reprints and permissions information is available at www.nature.com/reprints. The authors declare no competing financial interests. Readers are welcome to comment on the online version of the paper. Correspondence and requests for materials should be addressed to J.L.T. (turner@astro.ucla.edu).

METHODS

Submillimeter Array observations. NGC 5253 was observed with the Submillimeter Array (SMA)[31] on 2011 April 17. The observing frequency was $\nu_{LO} = 340.323$ GHz with 48 adjacent spectral windows covering 4 GHz bandwidth for each of two sidebands. The CO $J = 3 \rightarrow 2$ rotational transition at $\nu_0 = 345.79599$ GHz was in the upper sideband. The array was in the subcompact configuration covering the visibility baselines between 9 and 80 kλ corresponding to the angular scales between 29″ and 2″. The phase centre was $\alpha_{J2000} = 13\,h\,39\,min\,56.249\,s$, $\delta_{J2000} = -31^\circ\,38'\,29.00''$. Calibration and reduction were performed with MIRIAD[32]. The instrumental bandpass was corrected using the quasar 3C 279; complex gains were calibrated using the nearby quasar J1316−336; the flux density scale was determined from the planet model of Neptune. Continuum and line emission were separated using the task *UVLIN* by fitting a linear model to line-free channels. The result is a cube of 25 channels of 10 km s^{-1} and a continuum map with an effective bandwidth of 8 GHz, convolved to a beam 4″ × 2″, position angle = 0°, shown in Extended Data Fig. 1. Final noise levels were 3 mJy per beam in the continuum map, and 50 mJy per beam in the individual 10 km s^{-1} channels.

CSO SHARC observations. The 350-μm continuum observations were made with the SHARC camera[33] at the Caltech Submillimeter Observatory on 1999 January 11–12, with 225-GHz opacities around 0.035 and 0.075 for the respective dates. The data consist of 2.2 h of on-the-fly mapping with a ∼60″ chopping secondary at 4.132 Hz, and were reduced with CRUSH[34], using an enhanced implementation of the Emerson II deconvolution algorithm[35], which uses sky rotation to fill in the poorly sampled spatial frequencies of the dual-beam chop. CRUSH removes direct-current detector offset and correlated sky-noise residuals; flatfields detectors based on sky response; and performs noise weighting, whitening and despiking. The main beam is 9″ full width at half-maximum at 350 μm, but the image presented here was smoothed to 12.7″ resolution. From observations of Mars taken immediately before the SHARC observations, at a similar elevation, it is estimated that the pointing is good to ∼5″ root mean squared (r.m.s.). The systematic aperture flux calibration of the 350-μm image is estimated to be good to within 7% r.m.s.

Relation of NGC 5253 to M83 and distance. NGC 5253 is a dwarf spheroidal galaxy of the Cen A/M83 galaxy complex[36], with a stellar mass of $\sim 1.5 \times 10^8 M_\odot$ (ref. 37) and an estimated[38] total mass, including dark matter, about tenfold higher. It is close to the large spiral galaxy M83 in projection. However, the distance to M83, 4.8 Mpc (ref. 39), is significantly larger than the distance to NGC 5253, at 3.8 Mpc (ref. 40). The H I streamer system[24,25] in the halo of NGC 5253, from which the CO streamer seems to emanate, strongly suggests that this dwarf galaxy has had some encounter in its past, but M83 does not seem to be responsible.

Cloud D CO emission. The $J = 3$ level of CO corresponds to an energy E_u/k of 33 K, a temperature that begins to distinguish actively star-forming clumps from giant molecular clouds. Cloud D is bright in CO(3→2), but only weakly detected in CO(2→1) (ref. 3), and not at all in CO(1→0) (ref. 5). The total flux of CO(3→2) emission in the galaxy and streamer is 110 ± 20 Jy km s^{-1}, about 30% less than the single-dish flux[41]. This is a typical value for local galaxies, because the array configuration is insensitive to structures <30″ in extent; the value is consistent with the extended streamer emission and with the JCMT-SCUBA continuum image[42]. The CO(2→1) image is shown in Extended Data Fig. 2, overlaid on the SMA CO(3→2) image. CO(3→2) was not detected in previous SMA observations[11] because of insufficient signal-to-noise. Located at $\alpha_{J2000} = 13\,h\,39\,min\,55.943\,s \pm 0.003\,s$, $\delta_{J2000} = -31^\circ\,38'\,25.097'' \pm 0.05''$, the Cloud D CO(3→2) source is coincident to within ±0.5″ with the core of the supernebula as defined by high-brightness 7-mm free–free emission[43]. The CO(3→2) line centre is at a heliocentric velocity of 397.5 ± 0.6 km s^{-1} and the CO flux of Cloud D is 41 Jy km s^{-1}. The size of the CO source in the integrated intensity map deconvolved from the beam is 2.8″ × 1.5″ ± 7%, position angle 12° ± 1°. The slight northward extension is consistent with features seen[4,8,21,43,44] in free–free emission, but it is also in the same direction as the elongation of the beams for northern synthesis arrays for this source.

Cloud D virial mass. The width of the CO(3→2) line is $\sigma = 9.2 \pm 0.6$ km s^{-1}, based on a least-squares fit to a Gaussian line profile. We adopt a value for the radius of half the full width at half-maximum of the geometric mean of the deconvolved source size, using $M_{vir} = \alpha M_\odot v^2 r$, where $v = 2.35\sigma$ (in km s^{-1}) and r is in parsecs, with coefficients of $\alpha = 190$, for $\rho \approx r^{-1}$, adopted here, and $\alpha = 126$ for $\rho \approx r^{-2}$ and 210 for $\rho \approx r^0$ giving the uncertainty limits in M_{vir} (ref. 45). We assume that the cloud is turbulently supported against gravity and dispersion-dominated, as for Galactic giant molecular clouds[46,47]; inclination effects should therefore not be important. If Cloud D is not bound, or has flows that are super-gravitational, our estimate for the virial mass is an overestimate.

Supernebula stellar mass. The stellar mass is based on STARBURST99 (refs 48, 49) modelling with the following constraints. First, the 7-mm flux density of the supernebula is 47 ± 4 mJy for the central 2″ (refs 8, 43). From this we obtain a Lyman continuum rate of $N_{Lyc} = 7 \times 10^{52}$ s^{-1} for a nebula at 12,000 K (refs 50, 51). Second, the cluster age must be consistent with Bracket γ equivalent width of 255 Å (refs 10, 52) and mid-infrared ionic line ratios[53]. Third, the cluster must be old enough to have Wolf–Rayet (WR) stars, which would explain the WR spectral signatures[13,14,50,51,54,55]. Fourth, the cluster must have mass less than the virial mass of $1.8 \times 10^6 M_\odot$, which is also the maximum mass allowed by the [SIV] and Bracket α linewidths[56,57]. We considered both Geneva high and Geneva $v = 40\%$ breakup stellar models; the high-velocity models permit older cluster ages. The main parameter to vary in fitting the models is the lower mass cutoff to initial mass function (IMF). We consider cluster models with standard Kroupa IMFs with upper mass cutoffs of $150 M_\odot$, and top-heavy IMFs. Kroupa IMFs with stellar masses down to $0.1 M_\odot$ cannot give cluster ages sufficiently old to have both WR stars and the given N_{Lyc}, in view of the upper limit on the cluster mass. The IMF must be top-heavy: a cluster of $M_{stars} = 1.1^{+0.7}_{-0.2} \times 10^6 M_\odot$ requires a lower mass cutoff of $>3 M_\odot$. This cluster mass is consistent with previous estimates[58,59]. The Lyman continuum rate inferred from free–free emission may be less than the true value because of leakage from the H II region. In addition, dust can absorb as much as 50% of the ionizing photons in dense Galactic H II regions[60]; this could also increase the stellar mass. Studies of the extended ionized gas in NGC 5253 (ref. 61) indicate a total galactic star formation rate of twice what we calculate for the supernebula, but this could be ultraviolet photons from nearby slightly older clusters[27–29,58].

Cloud D continuum and dust mass. The strong 870-μm continuum source towards Cloud D consists of equal parts free–free emission from the H II region and dust emission. The continuum source is located at $\alpha_{J2000} = 13\,h\,39\,min\,55.948\,s \pm 0.005\,s$, $\delta_{J2000} = -31^\circ\,38'\,24.88'' \pm 0.11''$ (J2000). The 870-μm peak is 0.5″ north and 0.32″ west of the 7-mm continuum supernebula core[43], which is within the uncertainties of our 4″ × 2″ beam. The continuum source agrees in position and size with the CO source. The total 870-μm flux density of Cloud D is 72 ± 10 mJy. This flux is consistent with previous observations[11], and constitutes ∼40% of the total 870-μm flux of 192 mJy for the galaxy as determined from a JCMT/SCUBA map[42]. We extrapolate a free–free flux density from the 7-mm value of 47 ± 4 mJy (refs 8, 43), using the $S_\nu \propto \nu^{-0.1}$ spectrum of optically thin emission, giving $S^{ff}_{870\mu m} = 38 \pm 4$ mJy for Cloud D. The dust emission is then $S^{dust}_{870\mu m} = S_{870\mu m} - S^{ff}_{870\mu m} = 34 \pm 14$ mJy. This value is just consistent with the upper limit set at 1.3 mm (ref. 3). The SHARC flux is $S^{dust}_{350\mu m} = 3.7 \pm 0.5$ Jy, of which ∼1.0 ± 0.2 Jy originates in Cloud D.

The dust mass is dependent on the submillimetre dust opacity and dust temperature. We adopt the opacity of the Large Magellanic Cloud[12], extrapolating from $\kappa(160\,\mu m) = 16$ cm^2 g^{-1} and $\beta = 1.7$ to obtain $\kappa(870) = 0.9$ cm^2 g^{-1}. The 350-μm and 870-μm fluxes for Cloud D are consistent with $\beta = 1.7$. For dust temperature we adopt $T_{dust} = 45$ K based on IRAS Point Source Catalog fluxes[62]; $T_{dust} < 57$ K based on IRAS 60-μm flux. These values of temperature and opacity give $M_{dust} = (1.5 \pm 0.1) \times 10^4 M_\odot\,(T/45\,K)^{-1}$ for the dust mass of Cloud D, with the uncertainty based on the flux. Previous determinations of the dust mass in NGC 5253 were for the entire galaxy, including the streamer, based on the large-aperture JCMT/SCUBA[42] flux density; if scaled to our flux of 34 mJy for Cloud D only, these models[59,63] would give a dust mass of $M_{dust} \approx (2\text{–}3) \times 10^4 M_\odot$, consistent with a cooler dust temperature.

Dust yield from the cluster and GTD. The GTD estimated from our dust mass of $1.5 \times 10^4 M_\odot$ and our gas mass derived from virial and stellar masses is ∼47 (embedded cluster) or 120 (cluster outside cloud). Either is significantly lower than the value of 650 predicted[64] from scaling the Galactic value of 160 (ref. 65) to the metallicity of NGC 5253. We argue that the high dust mass is from *in situ* enrichment by the cluster. The Brackett γ equivalent width of 255 Å (refs 10, 52) indicates a cluster age consistent with the presence of WR activity, so mass loss is expected. If the original progenitor cloud had a mass of $\sim 2 \times 10^6 M_\odot$, there would initially have been $\sim 3{,}000 M_\odot$ of dust in Cloud D, one-fifth of the amount that we observe. From STARBURST99 models with $z = 0.004$, Geneva high-mass-loss stellar models, for a $1.1 \times 10^6 M_\odot$ cluster of age 4.4 Myr with an initial mass function of range $3\text{–}150 M_\odot$ and $\log N_{Lyc} = 52.84$, one would expect a yield in elements C, N, O, Mg, Si and Fe of $\sim 24{,}000 M_\odot$, of which an estimated 30–50% would be in the form of dust[65,66]. If the cluster is more massive or more top-heavy, the mass loss can be higher. The Geneva rotating models give yields that are lower but still sufficient to explain the dust mass. The optical spectrum of NGC 5253 does not yet reflect this localized enrichment: the metallicity of ∼0.25 solar is based on nebular lines[13,14] from the extended nuclear H II region, whereas the embedded star cluster is behind at least 16 magnitudes of extinction. However, the small CO linewidth suggests that what has been produced in the cloud has so far largely stayed in the cloud.

Cloud D excitation modelling. The CO(3→2) to CO(2→1) line ratio can be used to constrain gas density and temperature. Extended Data Fig. 2 demonstrates clear differences between the emission in Cloud D and the streamer. RADEX[6] was used to perform non-LTE modelling of the line ratios. We assumed a black-body radiation field and a column density of 10^{16} cm^{-2}, consistent with the observed brightness. Allowed values of density and kinetic temperature for the adopted value of $I_{32}/I_{21} = 2.25$ and the 1σ lower limit of 2.0 are shown in Extended Data Fig. 3. For the value of 2.25, the lower limit on the gas kinetic temperature is $T_K \approx 350$ K; however,

the ratio of 2.1 is within the uncertainties and would give $T_K > 200$ K. The indication of thermal ratios in the near-infrared H_2 line ratios[7] would also support a high temperature for this cloud.

Mass of Cloud D based on X_{CO}. X_{CO} masses are based on CO(1→0) emission, which has not been detected in Cloud D. Given that the CO emission is optically thin, it seems that the X_{CO} value[3] would underpredict the H_2 mass by a factor of ~8.

Streamer kinematics. The streamer has been detected previously in CO(1→0) and CO(2→1) (refs 3, 5). The emission is found at heliocentric velocities of 410–430 km s^{-1}, which is red-shifted by about 20 km s^{-1} with respect to the galaxy and the supernebula Cloud D. High-resolution VLA images[24] also detect H I emission coincident with this streamer. The streamer coincides with filamentary emission in nebular lines of oxygen[67] and sulphur[68]; it has been suggested that this is an 'ionization cone', possibly even due to an active galactic nucleus[68]. We suggest that this emission is due to leakage of photons from the starburst, which are ionizing the surface of the infalling streamer.

Streamer CO and dust properties and GTD. The CO(3→2) emission originates largely from a single cloud, Cloud 'C' (ref. 3). For its line strength of $I_{32} = 3.9 \pm 0.6$ K km s^{-1}, the ratio I_{32}/I_{21} is 1.0 ± 0.3. RADEX models of the ratio are consistent with optically thick and cooler gas, $T \approx 20$ K, with $n \approx 10^{3.5}$–10^4 cm^{-3} (Extended Data Fig. 3). The molecular mass of the streamer based on CO(2→1) (ref. 3) is $M_{H_2} = 2 \times 10^6 M_\odot$ for a Galactic conversion factor, $X_{CO} = 2 \times 10^{20}$ cm^{-2} (K km s^{-1})$^{-1}$. The virial mass is $3 \times 10^6 M_\odot$ (ref. 3). The 870-μm dust continuum emission follows the CO (Fig. 2). The 870-μm flux density of the streamer is 26 ± 8 mJy, which is all dust (Fig. 2). Adopting the dust opacity $\kappa(870\ \mu m) = 0.9$ cm^2 g^{-1} and dust temperature $T_d = 20$ K, we obtain a dust mass of $M_{dust} = 2.6 \times 10^4 M_\odot$. The streamer thus has GTD ≈ 120 using the virial mass for the gas mass. If the H I gas[24] is added, the total H + H_2 mass becomes $4.3 \times 10^6 M_\odot$, which gives GTD = 170. That the streamer is molecular gas, and—even more surprisingly—dense molecular gas, is difficult to understand. Molecular gas favours high-pressure environments[69] such as the midplanes of the central regions of spiral disks. Even though the filament seems to be in a low-pressure environment, it is not only molecular, but also dense. Models of the streamer as an example of a primordial cooling filament, in which the gas collapses towards the centre of the dark-matter potential, are able to produce the observed inflow rate of gas of ~0.1–0.2$M_\odot$ yr^{-1} but are unable to reproduce the formation of the observed giant molecular clouds[9]. The streamer may be previously enriched gas.

Cloud F. Cloud F, located about 5″ to the southwest of Cloud D, was not detected in previous CO observations[3,5]. Clouds D and F are the only two detected giant molecular clouds within NGC 5253 proper. Using the Galactic CO conversion factor and assuming optically thick emission, for the observed flux of 17 ± 6 Jy km s^{-1} we obtain a mass of $M_{H_2} \approx 4 \times 10^5 M_\odot$ for Cloud F.

Star-formation efficiency and cluster survival. The canonical value of $\eta = 50\%$ is from virial considerations for the survival of a bound cluster with mass loss on timescales less than the crossing time[70]. It is possible for a cluster to survive with lower efficiency, to ~30%, if the gas is lost slowly and the cluster expands[2,71].

31. Moran, J. M. & Ho, P. T. P. Smithsonian Submillimeter Wavelength Array. *Proc. SPIE* **2200,** 335–346 (1994).
32. Sault, R. J., Teuben, P. J. & Wright, M. C. H. in *Astronomical Data Analysis Software and Systems IV* (eds Shaw, R., Payne, H. E. & Hayes, J. J. E.) 433–436 (Astron. Soc. Pacif. Conference Series Vol. 77, 1995).
33. Wang, N. *et al.* A submillimeter high angular resolution bolometer array camera for the Caltech submillimeter observatory. *Proc. STT* **7,** 426–438 (1996).
34. Kovács, A. CRUSH: fast and scalable data reduction for imaging arrays. *Proc. SPIE* **7420,** 45–59 (2008).
35. Emerson, D. T. in *Multi-feed Systems for Radio Telescopes* (eds Emerson, D. T. & Payne, J. M.) 309–317 (Astron. Soc. Pacif. Conference Series Vol. 75, 1995).
36. Karachentsev, I. D. *et al.* The Hubble flow around the Centaurus A/M83 galaxy complex. *Astron. J.* **133,** 504–517 (2007).
37. Martin, C. L. The impact of star formation on the interstellar medium in dwarf galaxies. II. The formation of galactic winds. *Astrophys. J.* **506,** 222–252 (1998).
38. Persic, M., Salucci, P. & Stel, F. The universal rotation curve of spiral galaxies. I. The dark matter connection. *Mon. Not. R. Astron. Soc.* **281,** 27–47 (1996).
39. Radburn-Smith, D. J. *et al.* The GHOSTS survey. I. Hubble Space Telescope Advanced Camera for Surveys data. *Astrophys. J.* **195,** 18 (2011).
40. Sakai, S., Ferrarese, L., Kennicutt, R. C. Jr & Saha, A. The effect of metallicity on Cepheid-based distances. *Astrophys. J.* **608,** 42–61 (2004).
41. Meier, D. S., Turner, J. L., Crosthwaite, L. P. & Beck, S. C. Warm molecular gas in dwarf starburst galaxies: CO(3–2) observations. *Astron. J.* **121,** 740–752 (2001).
42. James, A., Dunne, L., Eales, S. & Edmunds, M. G. SCUBA observations of galaxies with metallicity measurements: a new method for determining the relation between submillimetre luminosity and dust mass. *Mon. Not. R. Astron. Soc.* **335,** 753–761 (2002).
43. Turner, J. L. & Beck, S. C. The birth of a super star cluster. *Astrophys. J.* **602,** L85–L88 (2004).
44. Turner, J. L., Ho, P. T. P. & Beck, S. C. The radio properties of NGC 5253 and its unusual HII regions. *Astron. J.* **116,** 1212–1220 (1998).
45. MacLauren, I., Richardson, K. M. & Wolfendale, A. W. Corrections to virial estimates of molecular cloud masses. *Astrophys. J.* **333,** 821–825 (1988).
46. Solomon, P. M., Rivolo, A. R., Barrett, J. & Yahil, A. Mass, luminosity, and line width relations of Galactic molecular clouds. *Astrophys. J.* **319,** 730–741 (1987).
47. Heyer, M. & Brunt, C. M. The universality of turbulence in Galactic molecular clouds. *Astrophys. J.* **615,** L45–L48 (2004).
48. Leitherer, C. *et al.* Starburst99: synthesis models for galaxies with active star formation. *Astrophys. J. Suppl.* **123,** 3–40 (1999).
49. Leitherer, C. *et al.* The effects of stellar rotation. II. A comprehensive set of STARBURST99 models. *Astrophys. J.* **212** (Suppl.), 18 (2014).
50. Walsh, J. R. & Roy, J.-R. Optical spectroscopic and abundance mapping of the amorphous galaxy NGC 5253. *Mon. Not. R. Astron. Soc.* **239,** 297–324 (1989).
51. Monreal-Ibero, A., Walsh, J. R. & Vílchez, J. M. The ionized gas in the central region of NGC 5253. 2D mapping of the physical and chemical properties. *Astron. Astrophys.* **544,** A60 (2012).
52. Davies, R. I., Sugai, H. & Ward, M. J. Star-forming regions in blue compact dwarf galaxies. *Mon. Not. R. Astron. Soc.* **295,** 43–54 (1998).
53. Martín-Hernandez, N. L., Schaerer, D. & Sauvage, M. High spatial resolution mid-infrared spectroscopy of NGC 5253: the stellar content of the embedded super-star cluster. *Astron. Astrophys.* **429,** 449–467 (2005).
54. Schaerer, D., Contini, T., Kunth, D. & Meynet, G. Detection of Wolf–Rayet stars of WN and WC subtypes in super-star clusters of NGC 5253. *Astrophys. J.* **481,** L75–L79 (1997).
55. Westmoquette, M. S., James, B., Monreal-Ibero, A. & Walsh, J. R. Piecing together the puzzle of NGC 5253: abundances, kinematics, and WR stars. *Astron. Astrophys.* **550,** A88 (2013).
56. Turner, J. L. *et al.* An extragalactic supernebula confined by gravity. *Nature* **423,** 621–623 (2003).
57. Beck, S. C. *et al.* [SIV] in the NGC 5253 supernebula: ionized gas kinematics at high resolution. *Astrophys. J.* **755,** 59 (2012).
58. Calzetti, D. *et al.* Dust and recent star formation in the core of NGC 5253. *Astron. J.* **114,** 1834–1849 (1997).
59. Vanzi, L. & Sauvage, M. Dust and super star clusters in NGC 5253. *Astron. Astrophys.* **415,** 509–520 (2004).
60. McKee, C. F. & Williams, J. P. The luminosity function of OB associations in the Galaxy. *Astrophys. J.* **476,** 144–165 (1997).
61. Martin, C. L. & Kennicutt, R. C. Jr. Soft X-ray emission from NGC 5253 and the ionized interstellar medium. *Astrophys. J.* **447,** 171–183 (1995).
62. Thronson, H. A. & Telesco, C. M. Star formation in active dwarf galaxies. *Astrophys. J.* **311,** 98–112 (1986).
63. Hunt, L., Bianchi, S. & Maiolino, R. The optical-to-radio spectral energy distributions of low-metallicity blue compact dwarf galaxies. *Astron. Astrophys.* **434,** 849–866 (2005).
64. Rémy-Ruyer, A. *et al.* Gas-to-dust ratios in local galaxies over a 2 dex metallicity range. *Astron. Astrophys.* **562,** A31 (2014).
65. Zubko, V., Dwek, E. & Arendt, R. G. Interstellar dust models consistent with extinction, emission, and abundance constraints. *Astrophys. J. Suppl.* **152,** 211–249 (2004).
66. Jenkins, E. B. A unified representation of gas-phase element depletions in the interstellar medium. *Astrophys. J.* **700,** 1299–1348 (2009).
67. Graham, J. Filamentary structure in NGC 5253. *Publ. Astron. Soc. Pacif.* **93,** 552–553 (1981).
68. Zastrow, J., Oey, M. S., Veilleux, S., McDonald, M. & Martin, C. L. An ionization cone in the dwarf starburst galaxy NGC 5253. *Astrophys. J.* **741,** L17 (2011).
69. Elmegreen, B. A pressure and metallicity dependence for molecular cloud correlations and the calibration of mass. *Astrophys. J.* **338,** 178–196 (1989).
70. Mathieu, R. D. Dynamical constraints on star formation efficiency. *Astrophys. J.* **267,** L97–L101 (1983).
71. Baumgardt, H., Kroupa, P. & Parmentier, G. The influence of residual gas expulsion on the evolution of the Galactic globular cluster system and the origin of the Population II halo. *Mon. Not. R. Astron. Soc.* **384,** 1231–1241 (2008).

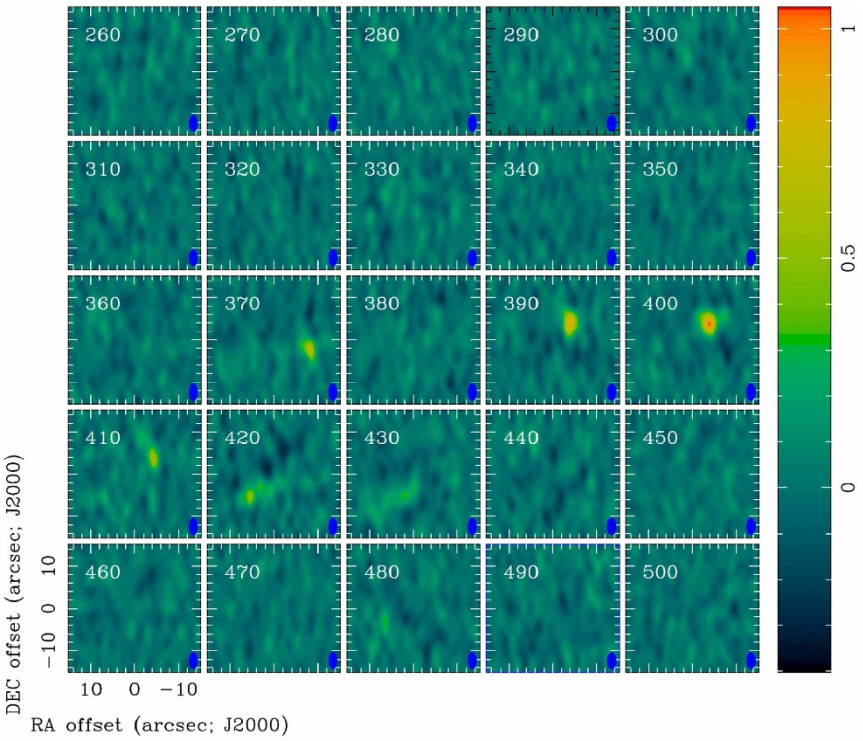

Extended Data Figure 1 | Channel maps of CO(3→2) emission in NGC 5253. Positions are relative to a reference position 13 h 39 m 56.249 s, −31° 38′ 29″ (J2000). Channels are 10 km s^{-1} wide; the heliocentric velocity is noted on the individual maps. The colour bar range maximum is 1 Jy per beam for each 10 km s^{-1} channel. The beam is 4″ × 2″, p.a. 0°.

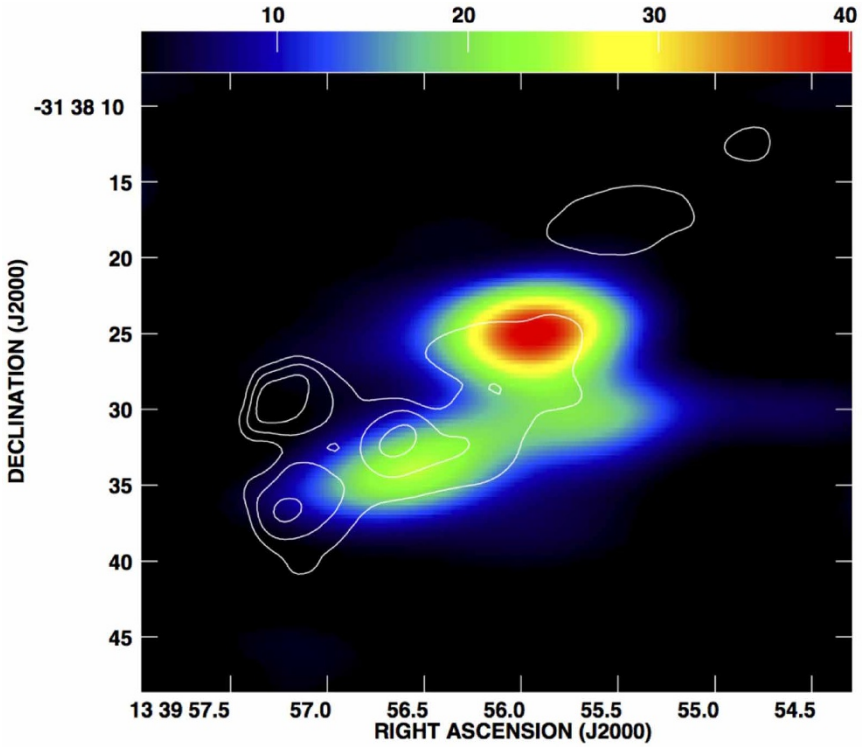

Extended Data Figure 2 | SMA image of CO(3→2) with CO(2→1). CO(3→2) emission is shown in colour, with an image[2] from the Owens Valley Millimeter Array of CO(2→1) in contours. The SMA CO(3→2) image has been smoothed from its original $4'' \times 2''$, p.a. 0° resolution to match the $9.7'' \times 5''$, p.a. -84°, beam of the CO(2→1) image. The colour image flux range is 3–40 Jy km s^{-1} per beam. Contours are linear multiples of 4 Jy km s^{-1} per beam.

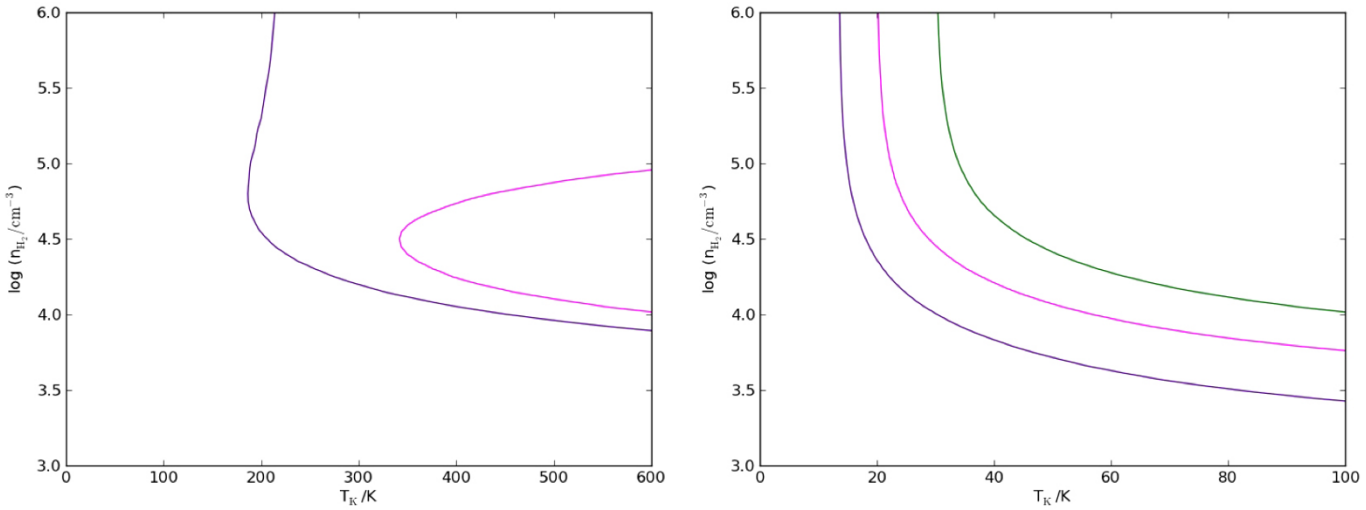

Extended Data Figure 3 | RADEX modelling of Cloud D and streamer. Escape probability transfer modelling of the CO(3→2) to CO(2→1) line ratio. Models were run using a black-body radiation field, spherical escape probability and $N_{CO} = 10^{16}$ cm^{-2}. **a**, Cloud D. Magenta is for the value $I_{32}/I_{21} = 2.25$, the optically thin limit, and indigo is for the 1σ lower limit to the measured value of 2.6. There is no solution for $I_{32}/I_{21} = 2.6$. **b**, Streamer. Magenta is for $I_{32}/I_{21} = 0.98$, and indigo and green are solutions for the -1σ and $+1\sigma$ values, respectively.